Virtual and Experimental Visualization of Flows in Packed Beds of Spheres Simulating Porous Media Flows

R.C. Hendricks
Lewis Research Center, Cleveland, Ohio

M.M. Athavale
CFD Research Corporation, Huntsville, Alabama

S.B. Lattime
B&C Engineering, Akron, Ohio

M.J. Braun
University of Akron, Akron, Ohio

The NASA STI Program Office . . . in Profile

Since its founding, NASA has been dedicated to the advancement of aeronautics and space science. The NASA Scientific and Technical Information (STI) Program Office plays a key part in helping NASA maintain this important role.

The NASA STI Program Office is operated by Langley Research Center, the Lead Center for NASA's scientific and technical information. The NASA STI Program Office provides access to the NASA STI Database, the largest collection of aeronautical and space science STI in the world. The Program Office is also NASA's institutional mechanism for disseminating the results of its research and development activities. These results are published by NASA in the NASA STI Report Series, which includes the following report types:

- TECHNICAL PUBLICATION. Reports of completed research or a major significant phase of research that present the results of NASA programs and include extensive data or theoretical analysis. Includes compilations of significant scientific and technical data and information deemed to be of continuing reference value. NASA's counterpart of peer-reviewed formal professional papers but has less stringent limitations on manuscript length and extent of graphic presentations.

- TECHNICAL MEMORANDUM. Scientific and technical findings that are preliminary or of specialized interest, e.g., quick release reports, working papers, and bibliographies that contain minimal annotation. Does not contain extensive analysis.

- CONTRACTOR REPORT. Scientific and technical findings by NASA-sponsored contractors and grantees.

- CONFERENCE PUBLICATION. Collected papers from scientific and technical conferences, symposia, seminars, or other meetings sponsored or cosponsored by NASA.

- SPECIAL PUBLICATION. Scientific, technical, or historical information from NASA programs, projects, and missions, often concerned with subjects having substantial public interest.

- TECHNICAL TRANSLATION. English-language translations of foreign scientific and technical material pertinent to NASA's mission.

Specialized services that complement the STI Program Office's diverse offerings include creating custom thesauri, building customized data bases, organizing and publishing research results . . . even providing videos.

For more information about the NASA STI Program Office, see the following:

- Access the NASA STI Program Home Page at *http://www.sti.nasa.gov*

- E-mail your question via the Internet to help@sti.nasa.gov

- Fax your question to the NASA Access Help Desk at (301) 621-0134

- Telephone the NASA Access Help Desk at (301) 621-0390

- Write to:
  NASA Access Help Desk
  NASA Center for AeroSpace Information
  7121 Standard Drive
  Hanover, MD 21076

Virtual and Experimental Visualization of Flows in Packed Beds of Spheres Simulating Porous Media Flows

R.C. Hendricks
Lewis Research Center, Cleveland, Ohio

M.M. Athavale
CFD Research Corporation, Huntsville, Alabama

S.B. Lattime
B&C Engineering, Akron, Ohio

M.J. Braun
University of Akron, Akron, Ohio

National Aeronautics and
Space Administration

Lewis Research Center

August 1998

Available from

Virtual and Experimental Visualization of Flows in Packed Beds of Spheres Simulating Porous Media Flows

R.C. Hendricks[1], M.M. Athavale[2], S.B. Lattime[3], M.J. Braun[4]

Abstract

A videotape presentation of flow in a packed bed of spheres is provided. The flow experiment consisted of three principal elements: (1) an oil tunnel 76.2 mm by 76.2 mm in cross section, (2) a packed bed of spheres in regular and irregular arrays, and (3) a flow characterization methodology, either (a) full flow field tracking (FFFT) or (b) computational fluid dynamic (CFD) simulation. The refraction indices of the oil and the test array of spheres were closely matched, and the flow was seeded with aluminum oxide particles. Planar laser light provided a two-dimensional projection of the flow field, and a traverse simulated a three-dimensional image of the entire flow field. Light focusing and reflection rendered the spheres black, permitting visualization of the planar circular interfaces in both the axial and transverse directions. Flows were observed near the wall-sphere interface and within the set of spheres.

The CFD model required that a representative section of a packed bed be formed and gridded, enclosing and cutting six spheres so that symmetry conditions could be imposed at all cross-boundaries. Simulations had to be made with the flow direction at right angles to that used in the experiments, however, to take advantage of flow symmetry. Careful attention to detail was required for proper gridding. The flow field was three-dimensional and complex to describe, yet the most prominent finding was flow threads, as computed in the representative 'cube' of spheres with face symmetry and conclusively demonstrated experimentally herein. Random packing and bed voids tended to disrupt the laminar flow, creating vortices.

Nomenclature

A	area
D	sphere diameter
Go	mass flux (no spheres in tunnel)
L	length, model of spheres
Δp	pressure drop
Re	Reynolds number
V	volume
x,y,z	coordinates
ε	volume porosity
ρ	density
μ	viscosity

Introduction

Although similar visualization materials and techniques have been discussed in previous work by Hendricks [1,2], it was realized that printed frames, grabbed from videotapes of the flows in beds of packed spheres failed to reproduce what was visualized either in computational fluid dynamic (CFD) virtual images or experimentally. And herein, the essences of the numerical and experimental work are synergistically combined to provide background for the visualization that can be realized only by viewing the videorecording (of the experiment or the CFD virtual images) or the experiment itself.

Packed spherical particle beds are characterized, for example, by Ergun [3] and Bird et al. [4] as empirical combinations of laminar and turbulent flows. Process design engineers use similar methods to define packed beds of spheres for a wide variety of porous media applications (filters, catalytic packs, heat exchangers, etc.). Yet the details of heat, mass,

---

[1]NASA Lewis Research Center, Cleveland, Ohio 44135, USA
[2]CFD Research Corp., Huntsville, Alabama 35805, USA
[3]B&C Engineering, Akron, Ohio 44311, USA
[4]University of Akron, Akron, Ohio 44325, USA

and momentum transfers in these packed structures are not understood. Studies made of a dumped bed of spheres by Jolls and Hanratty [5] and confirmed by Karabelas [6] show that the flow is three-dimensional and laminar at Reynolds numbers (Re) less than 40, with unsteady flows occurring at $110 < Re < 150$. Flows in cubic arrays of spheres are steady to $Re = 82$ and characterized by nine regions of reverse flow with similar patterns observed for $Re = 200$, even though the flow becomes unsteady [7]. In numerical modeling of porous media Saleh et al. [8], Rosenstein [9], and Yarlagadda and Yoganathan [10] found that little knowledge of the interstitial flow fields was available. Saleh used particle image planar displacement velocimetry and integration of the continuity equation to describe the third component (similar to the procedure used by Rosenstein).

The full flow field tracking (FFFT) method [11,12] can be applied to visualize and quantize the flow patterns and fluid velocities within a packed bed of spheres. The numerical simulations were made with the code SCISEAL, a pressure-based, finite-volume, three-dimensional CFD code with implicit multiple-block capability [13]. More

details of packed-bed sphere flows can be found in Athavale et al. [14]. The gridding was executed by using CFD-GEOM [15]. Materials from Athavale et al. [13,14] and Hendricks et al. [1,2] are used to orient the reader in viewing the videotape.

Test Facility

The test facility consisted of an oil tunnel, flow system components, videorecording equipment, a 4-W continuous-wave (4CW) argon-ion laser, lens systems, data recorders, and a test configuration (fig. 1). The matrix of spheres (fig. 2) and entry ramp spacer was fabricated to fill the tunnel cross section (76.2 mm by 76.2 mm). Both the laser light sheet and the viewing port walls were Lucite. The test sphere matrix was fabricated by using optical quality glue to bind the array, matching the refraction index of Lucite, 1.4905. This technique sacrificed the point of contact, yet permitted construction of a regular array of staggered spheres and a clear view through the spheres when they were immersed in the oil, which also had the same refraction index as Lucite. The spheres in the bottom layer were ground flat, and their height was ad-
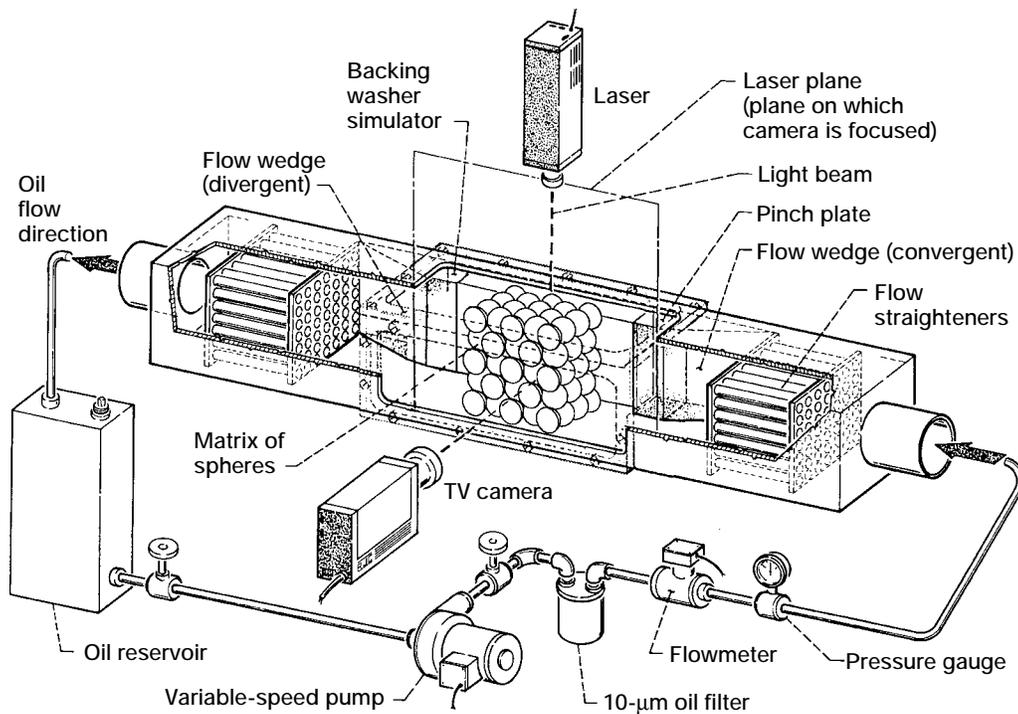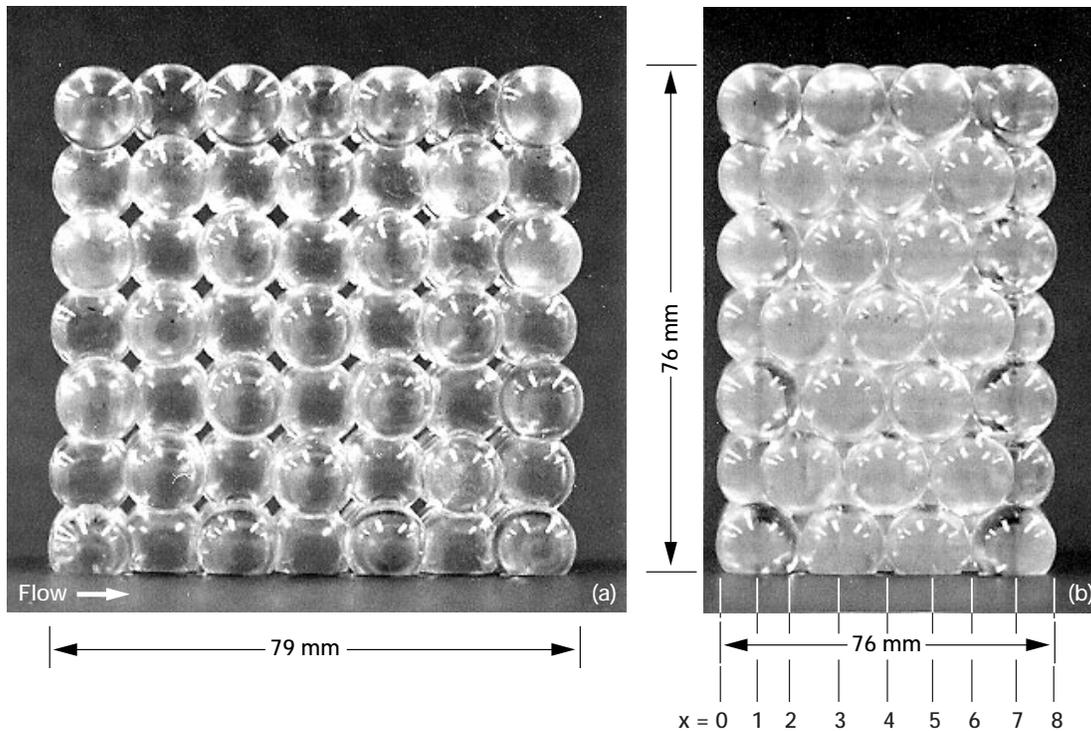

Figure 1.—Schematic of test facility.

Figure 2.—Matrices of Lucite spheres of refractive index 1.4905; sphere diameter, 12.7 mm. x = 0(front wall), x = 1 (6.4 mm), x = 2 (12.7 mm), x = 3 (19.1 mm), x = 4 (midplane). (a) Side view (camera view). (b) Front view (flow view).

justed to exactly fit the tunnel. No other spheres were altered. The width was adjusted by using a gradual entry ramp that blocked a portion of the tunnel and at the same time eliminated any recirculating flow at the entry of the array.

The packed sphere bed (78.7 mm long by 50.8 mm wide by 76.2 mm high) contained 172 spheres. The 7-by-7 longitudinal array (fig. 2(a)) had a transverse array of four 12.7-mm-diameter spheres (fig. 2(b)). The volume of the test array envelope was $V_t = 305$ cm^3, the solid volume of spheres was $V_s = 184$ cm^3. The void $V_o = V_t - V_s = 121$ cm^3, with an effective open cross section for flow of $A_e = 17.9$ cm^2. The geometric arrangements for the numerical analysis and sphere identification are given as figures 6 and 7 and discussed later.

The coherent beam of the 4CW argon-ion laser was directed by micrometrically adjustable mirrors through two cylindrical lenses positioned at 90° to each other, through the Lucite tunnel window, and into the test section. The light sheet was approximately 0.1 mm thick, and the flow was seeded with

magnesium oxide flow tracers. Micrometric adjustments controlled the position of the light slices scanning across the test section and provided, through composition, a three-dimensional visualization of the flow field. The light was naturally focused and reflected at the boundary interfaces between the working fluid and the spheres, rendering the spheres black and permitting visualization of the planar circular interfaces in both the axial and transverse directions. The images were recorded on a videocassette recorder.

Other instrumentation included static pressure taps and thermocouples upstream and downstream of the test matrix and two spheres coated with liquid crystal with a narrow band response about 21 °C.

Experimental Results

Figure 3 represents the flow field 6.35 mm from the front window ($x = 1$) in the array of 12.7-mm-diameter spheres. The flow rate was 3.8 l/min (1 gal/min). The spheres were numbered to facili-
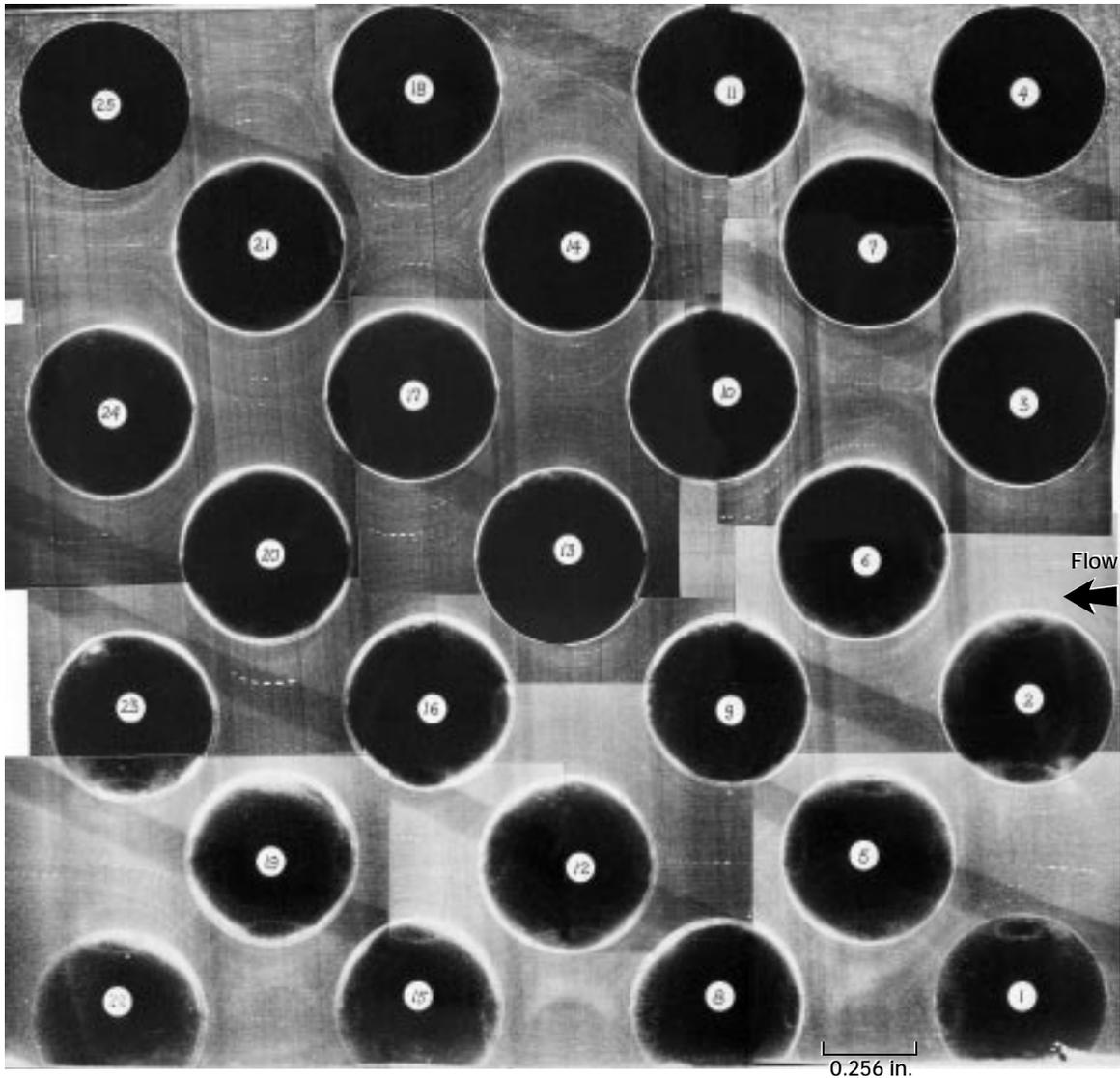
Figure 3.—Visualization of flow in 12.7-mm-diameter sphere matrix (fig. 2) 6.4 mm from front wall (x = 1.0) with flow at 3.8 liters/min (1 gal/min).

tate flow descriptions. The laser light slice was strobed at 180 Hz, giving a six-segment particle streak per recorded videotape frame. The inlet flow streaks around spheres 1 to 4 resemble flows around an array of cylindrical pins. Stagnation zones occurred in front of and behind spheres 1 to 4, and wake zones appeared behind spheres 22 to 25. Flow near the tunnel upper wall, spheres 4, 11, 18 and 25, showed a high level of distortion and lower velocities, illustrating the influence of a sphere-wall boundary. Careful attention to the particle trace lengths and brightness defined a flow thread in the axial direction, which for regular arrays resembled

a complex sine wave. The flow spiraled upward from the gap between spheres 13 and 16, then slowed and turned downward into the pocket formed by spheres 16, 19, 20, and 23, and flowed out between spheres 20 and 23. The streak between spheres 1 and 2 headed to the stagnation zone of sphere 5. The wake of sphere 5 was vivid and a streak extended toward the stagnation zone of sphere 12. The wake behind sphere 14 and the stagnation zone in front of sphere 21 were almost connected. Flow symmetry existed between spheres 10, 13, 14, and 17 and the closing of small wakes behind spheres 2 and 3. The flow thread was complex.
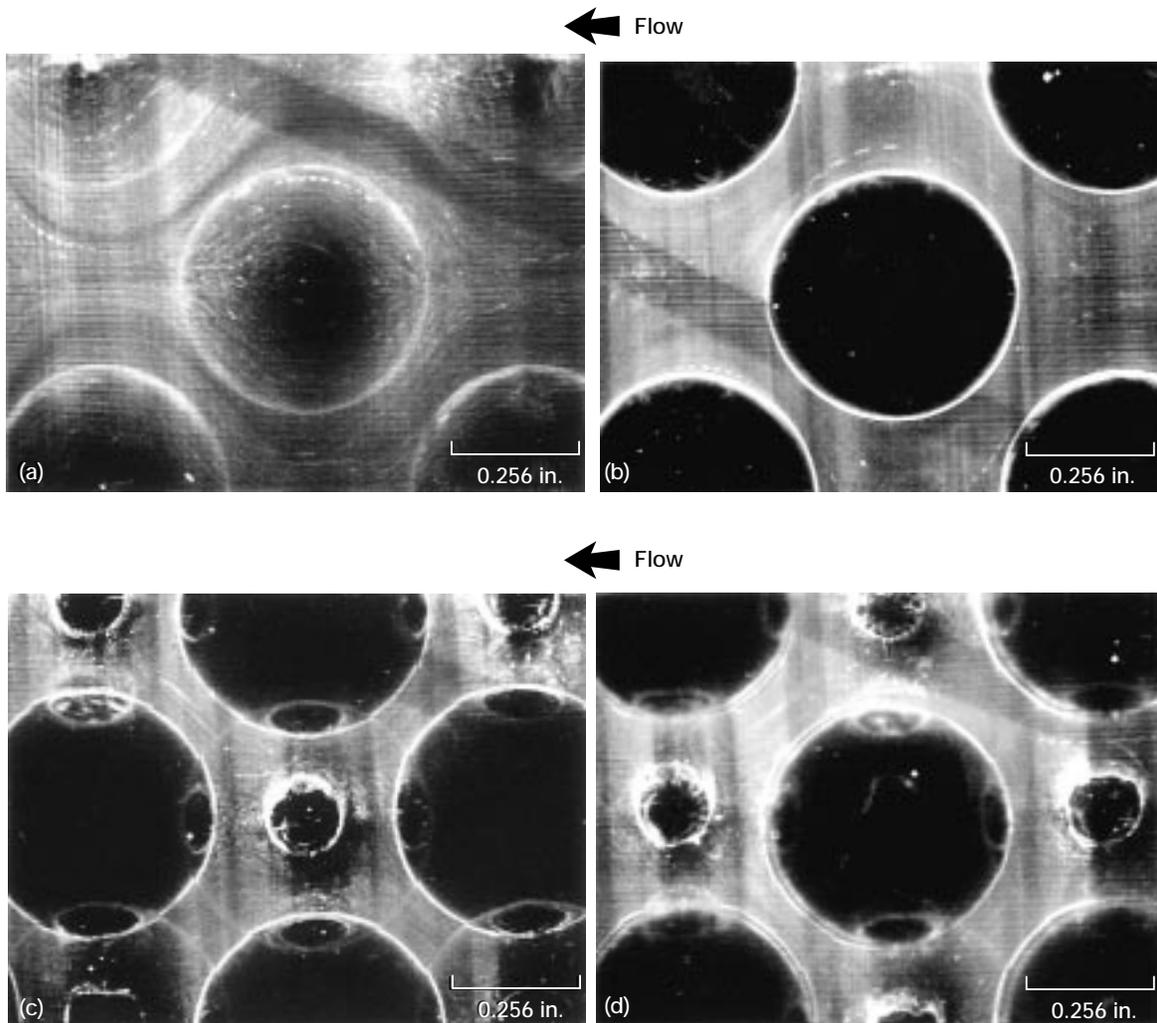
Figure 4.—Transverse visualization of flow in 12.7-mm-diameter sphere matrix (fig. 2) at column of spheres 5, 6, and 7 (fig. 3) with flow at 11.4 liters/min (3 gal/min). (a) $x = 0$ (front wall). (b) $x = 1$ (0.5 sphere diameter from wall). (c) $x = 2$ (1 sphere diameter from wall). (d) $x = 3$ (1.5 sphere diameters from wall).

Midway across the matrix block, 25.4 mm from the front wall ($x = 4$), the effects of the upper wall on the flow between spheres 11, 14, 18, 21, and 25 was still pronounced, with diminished velocities between spheres 18, 21, and 25 and the wall.

At 11.4 l/min (3 gal/min) the boundary layers, jetting, and wakes became more pronounced. Figure 4 is a transverse scan of flow that includes the column of spheres 5, 6, and 7 (see figs. 2 and 3). Figure 4(a) shows low-velocity flow streaks and threads about the sphere in the immediate vicinity of the front lateral wall ($x = 0$). Figure 4(b) shows higher velocity flow streaks at $x = 1.0$ (6.4 mm, or 0.5 sphere diameter), and particles tracking the

weaving flow thread are partially visible. In figure 4(c), at $x = 2$ (12.7 mm, or 1 sphere diameter), the light sheet is skewed and portions of the adjacent spheres and their multiple contact points become visible. Figure 4(d), at $x = 3$ (19.1 mm, or 1.5 sphere diameters), shows the flow thread around a sphere and adjacent contact points.

Figure 5 presents a closeup view of the flow in the upper part of figure 4(d) at a magnification of 7.8. The strong effects of the flow are apparent from a stagnation region in the cusp at the confluence between the spheres and the extremely slow flow in the channel between the spheres.
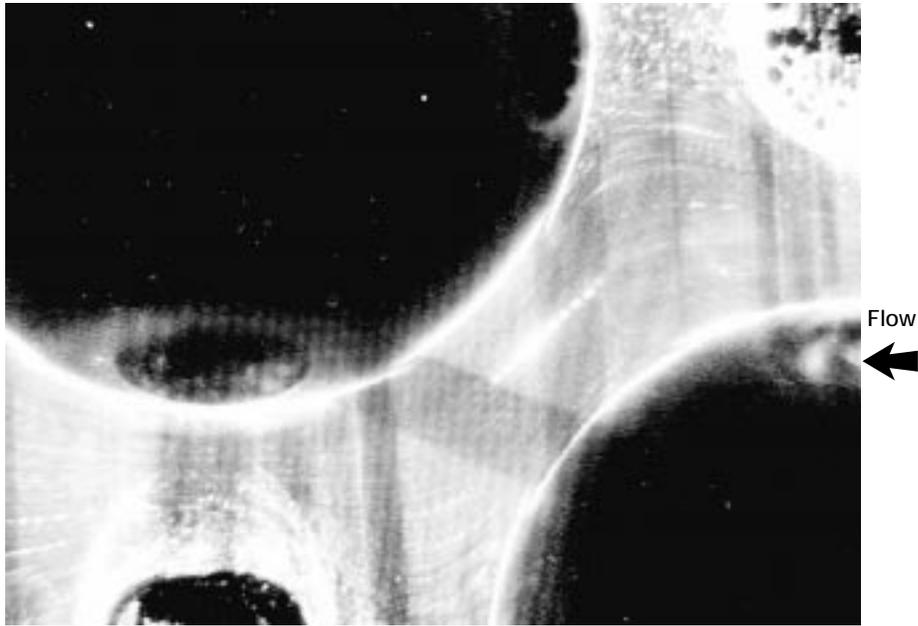
Figure 5.—Sphere matrix flow image at 7.8X for 12.7-mm-diameter sphere matrix and 11.4-liters/min (3-gal/min) flow rate.
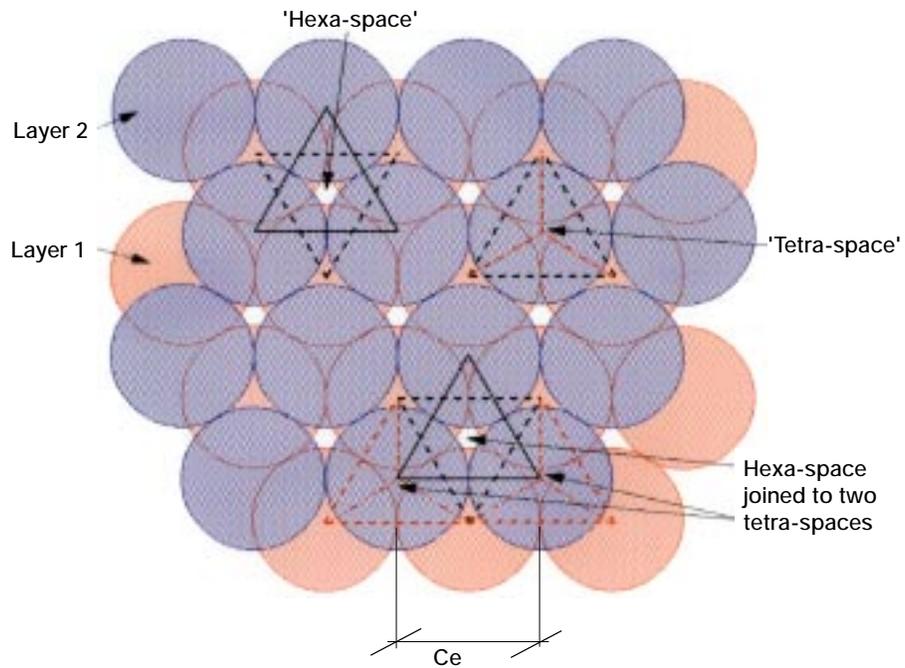

Figure 6.—Stacking of sphere layers to generate densely packed arrangements.

Numerical Modeling

Unlike visualization of flows in pinned arrays, which are weakly three-dimensional dependent, the flow, heat, and mass transfers in spherical beds are strongly three-dimensional dependent and require the combined efforts of numerical and experimental techniques to embody and characterize models and results. Also in contrast to pinned arrays, the geometric descriptions become quite complex. Spherical clusters with hexagonal or cubic densely packed beds have 12 neighbors and a void fraction of about 0.26 (figs. 6 and 7). The first-ever simulations of the flow in the interstitial spaces of a hexagonal densely packed arrangement were done by Athavale et al. [14] using structured, multiple-domain grids. Two types of interstitial space were identified as the basic building blocks for generating the flow by replication. The two types were (1) tetra-space, bounded by four spheres with centers at the apex of a tetrahedron; and (2) hexa-space, bounded by six spheres with centers at the apexes of a double pyramidal structure. Each of these spaces was further subdivided into simpler domains so as to be able to build structured grids in the flow domain. By joining the tetra- and hexa-spaces at appropriate planes, a given volume could be populated with the closely packed spheres. Flow and heat transfer simulations on these spheres were reported by Athavale et al. [14]. The complexity of the flow domain, however, limited the overall domain size that could be considered with structured grids. The number of domains and grid cells grew rapidly with each tetra- and hexa-space added to the flow problem. Additionally, each space contained a singularity point, and the grid topology often forced grid clustering in areas where it was not needed, leading to nonoptimal use of the available cells.

With an unstructured grid format, where the basic volume element is a tetrahedron, the complex shapes of the interstitial spaces could be gridded more easily, with better control of surface and volume discretization in terms of cell sizes and clustering. In addition, with the unstructured grid

---

[1]For identifying the basic spaces ping-pong balls are useful mnemonics.

format the representative 'slice' of the flow domain could be easily created by using much simpler cutting planes (e.g., parallel to *xy*, *yz*, and *zx* planes in the Cartesian coordinate system) rather than the naturally occurring interfaces that had to be used with the structured grids. Finally, by using proper cutting planes and locations, symmetry and periodicity boundaries could be used to make the flow in the representative slice close to the real situation in a packed bed.

Figure 8(a)[1] shows a solid model of such a representative slice, with surface triangulation on all outer boundary surfaces (fig. 8(b)). The curved surfaces are all outer surfaces of the bounding spheres and are no-slip walls. The planar surfaces in between are the areas where flow can take place. With this grid orientation, for a direct comparison with the experiments, the bulk flow should be along the *z* direction. However, because the *xz* plane surfaces are not in appropriate geometric locations for symmetry conditions, the flow direction was oriented along the *y* direction to allow the use of symmetry conditions on the cross-plane surfaces (*yz* and *yx* planes), which are identified in figure 8(a). With this change the viewing plane still remained the same (*yz* plane), but the flow direction in the simulations was at right angles to the experimental direction. Differences in the numerical and experimental cube of spheres are shown sketched in figures 9(a) and 9(b) respectively with tabulated porosities listed in table I. Although this prevented a direct comparison with the experiments, the simulations still showed a great deal of similarity with the experiments and offered insight into the complexity of the flow field. To allow bulk flow in the *z* direction, periodic conditions would need to be imposed in all three directions, and this work is under way.

The main flow direction, then, is along the *y* coordinate axis as shown. A uniform flow velocity was prescribed on the 'open' areas of the inlet *xz*

Table I.—Porosities of numerical and experimental cube of spheres models.

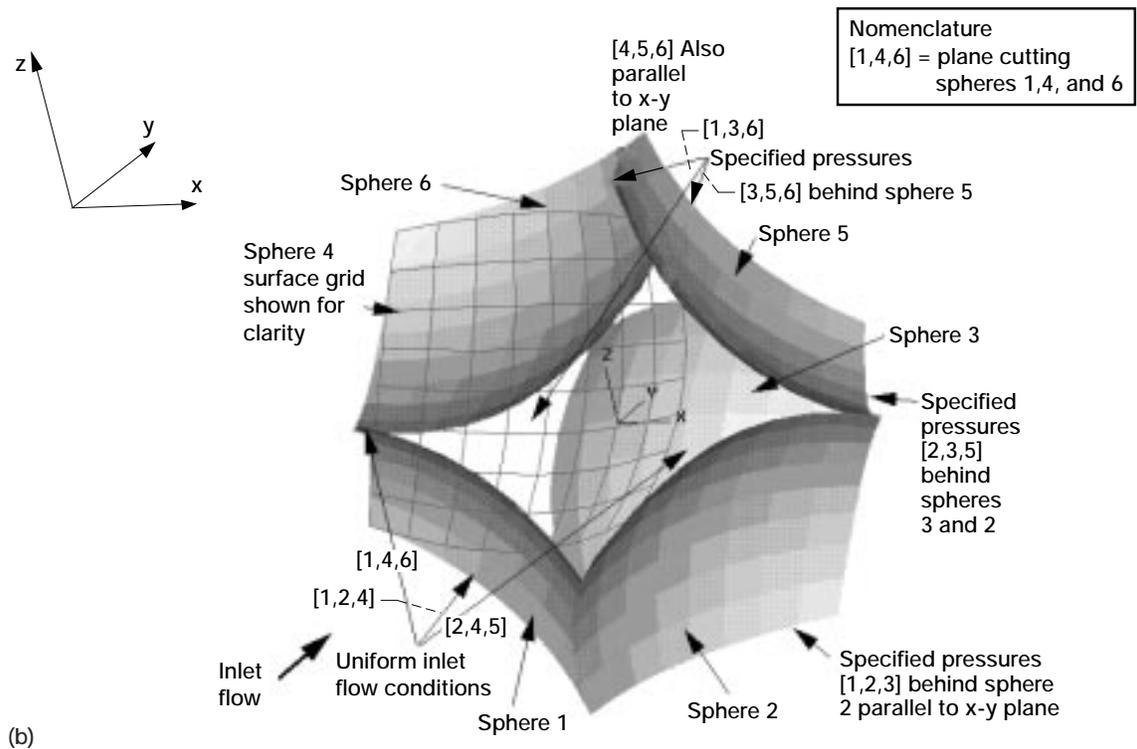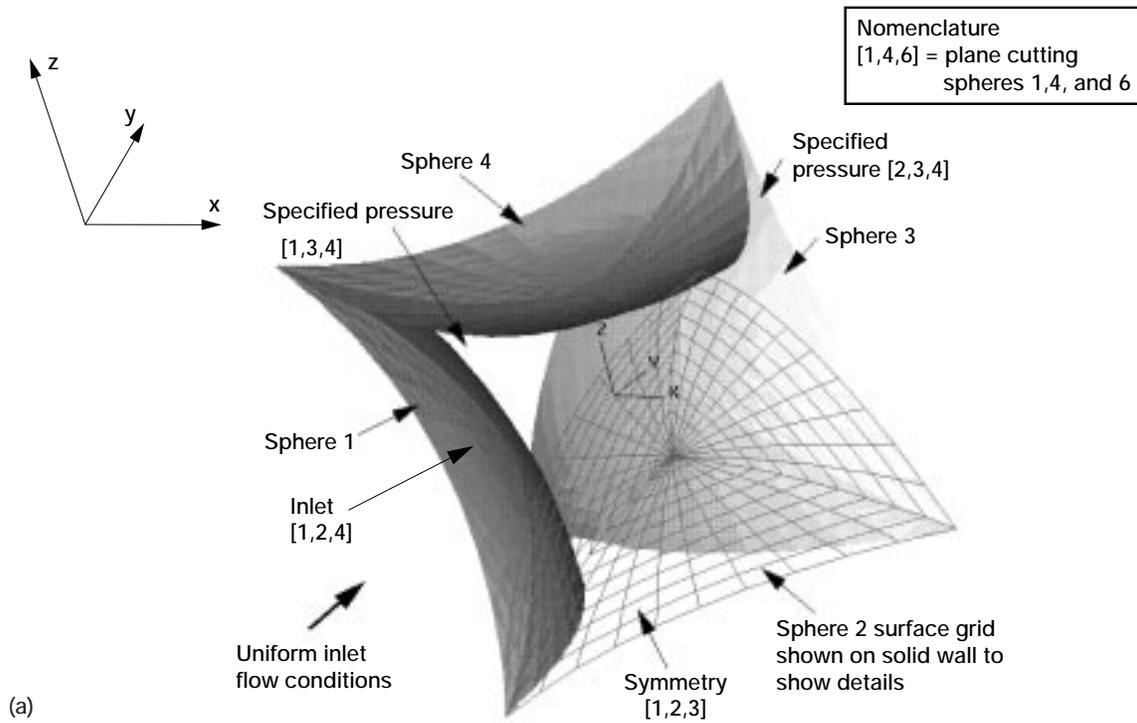| Volume porosity, Face porosity	Numerical	Experimental
	0.260	0.302
xy	0.093	0.093
xz	.198	.093
yz	.444	.476

Figure 7.—Solid model, showing flow geometry and boundary conditions. (a) Single tetra-space. (b) Single hexa-space.
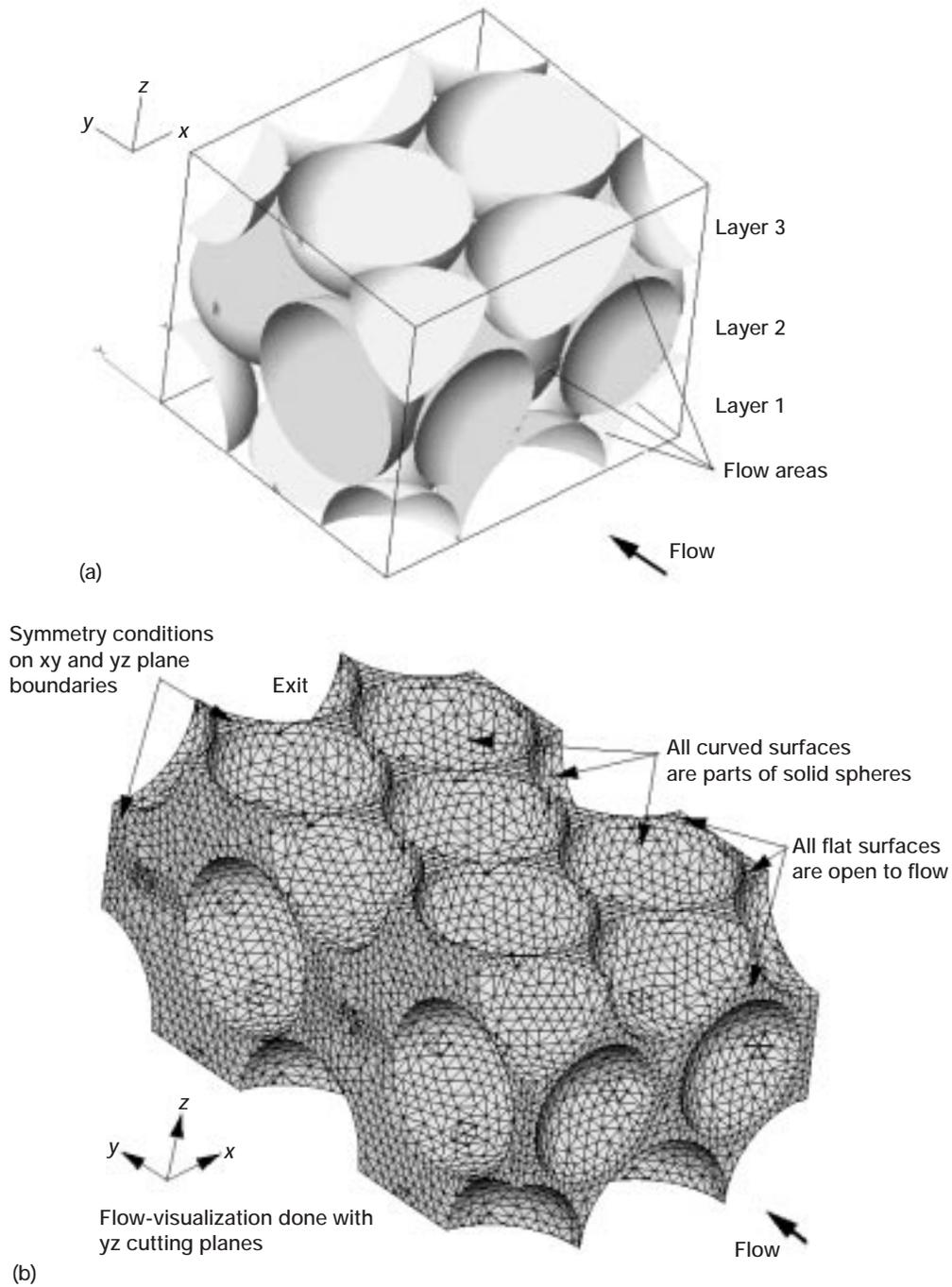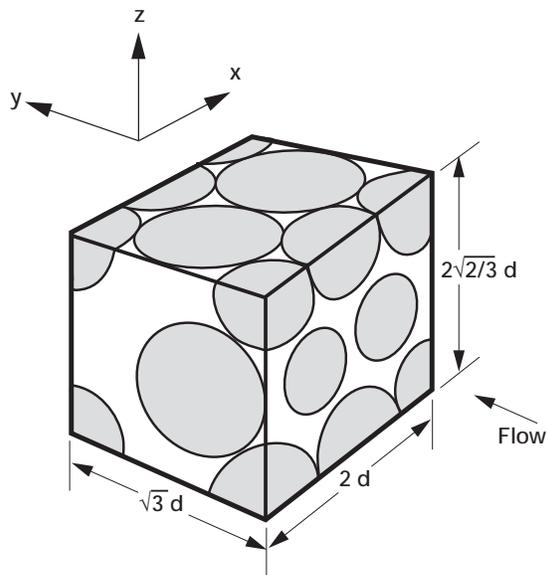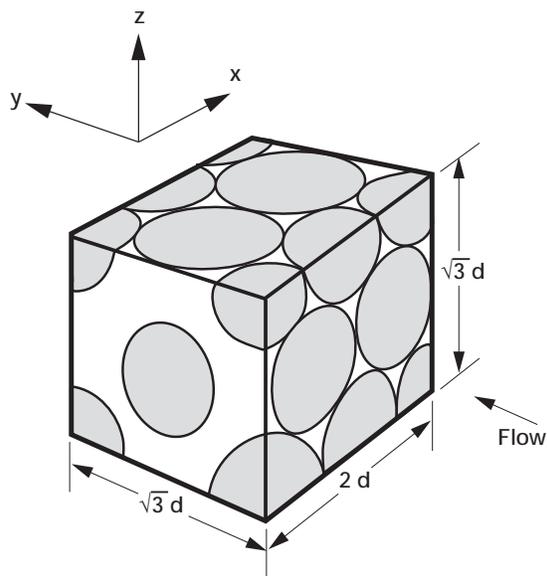
(a)

(b)

Figure 8.—Representative 'cube' in hexagonal densely packed arrangement of spheres. (a) Solid model. (b) Surface gridded two 'cube' model.

Figure 9.—'Cube' of spheres sketches. (a) Numerical. (b) Experimental.

plane, and a constant static pressure was specified at the opposite xz plane, the exit boundary. The uniform velocity and pressure values specified on the xz boundaries introduce 'entry' effects into the flow field for the flow Reynolds numbers consid-

ered. However, these effects were expected to last over a small distance inward from these two boundaries, and the flow in the central portion of the domain can be compared with that in the experiments.

Incompressible, constant-property, laminar flow[2] of oil through the matrix was simulated at the two volume flow rates used in the experiments. The inlet velocities corresponded to flow rates of 3.8 and 11.4 l/min (1 and 3 gal/min) in the test apparatus described above. The sphere diameters were set to 12.7 and 19.05 mm. The oil had a density of 900 kg/m^3 and a kinematic viscosity of 1.0×10^{-4} m^2/s. The free tunnel inlet velocities (no spheres in the tunnel) were 0.016 and 0.048 m/s, respectively, and adjusted by the flow cross-sectional area (with spheres in the tunnel) to yield the flow rates used in the analysis; $A_{total}/A_{open}|_{y=0} = 5.04$.

These and other flow rates are discussed in Numerical Results.

The flow solver used for simulations was SCISEAL(U), which has unstructured/hybrid grid capability. The code uses a pressure-based, finite-volume integration method to solve Navier-Stokes equations. It can be used to treat compressible and incompressible flows and has a variety of boundary condition types and conjugate heat transfer and turbulence models [13].

Numerical Results

Figures 10(a) and (b) are representative velocity vector plots within the array of spheres at two constant x planes for a flow rate of 3.8 l/min (1 gal/min). The orientation and magnitude of the velocity formed the flow thread as the yz cutting plane was moved one sphere diameter across the flow field (experimental flow is along the vertical direction in these figures). Although flow orientation, grid refinement, and postprocessing of the results require further resolution, initial values of the numerical pressure drop across the 'dual cube' were comparable to those calculated from the Ergun relation [3,4] (table II and fig. 11). Approximate average values of the static pressures over the inlet and outlet planes were used to calculate the pressure drop over the 'dual cube' and then normalized with the length of the flow domain in the flow direction to get the linear pressure drop rates.
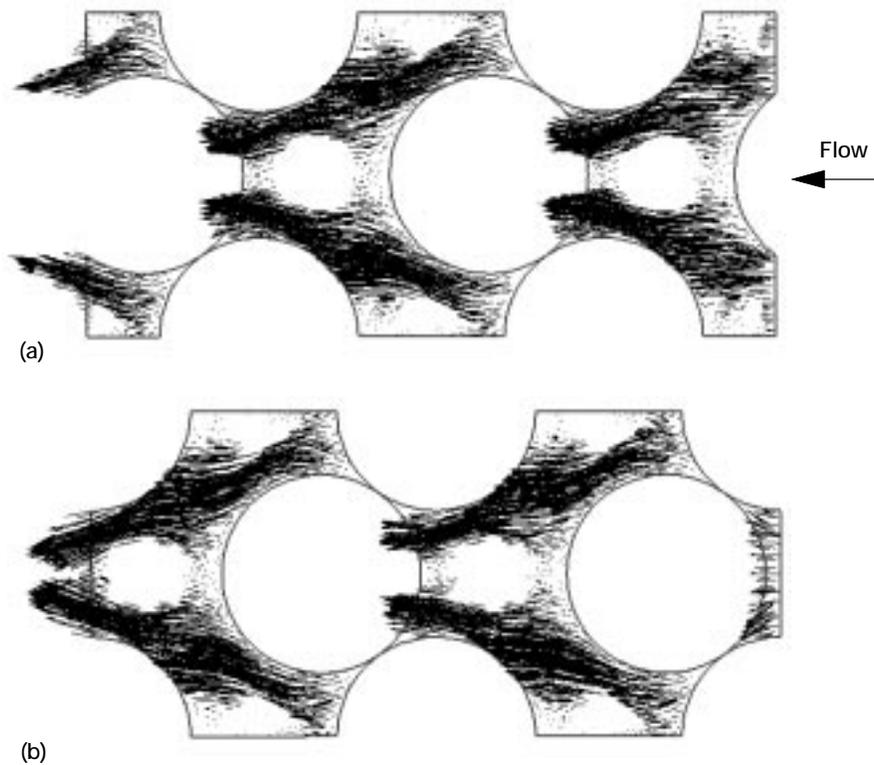
---

[2]It has been shown that for an absolutely regular, low-porosity (tightly packed) array of cylinders turbulence can not be engendered [16].

Figure 10.—Velocity vectors in single-axis hexa-space along yz (x = constant) cutting plane in sphere cluster with flow rate at 3.8 liters/min (1 gal/min). (a) x = 4. (b) x = 5.

Table II.—Comparison of numerical and calculated Ergun [3,4] pressure drops across arrays of spheres (Ergun parameters: porosity = 0.26, density = 900 kg/m^3, viscosity = 0.0904 Pa-s).

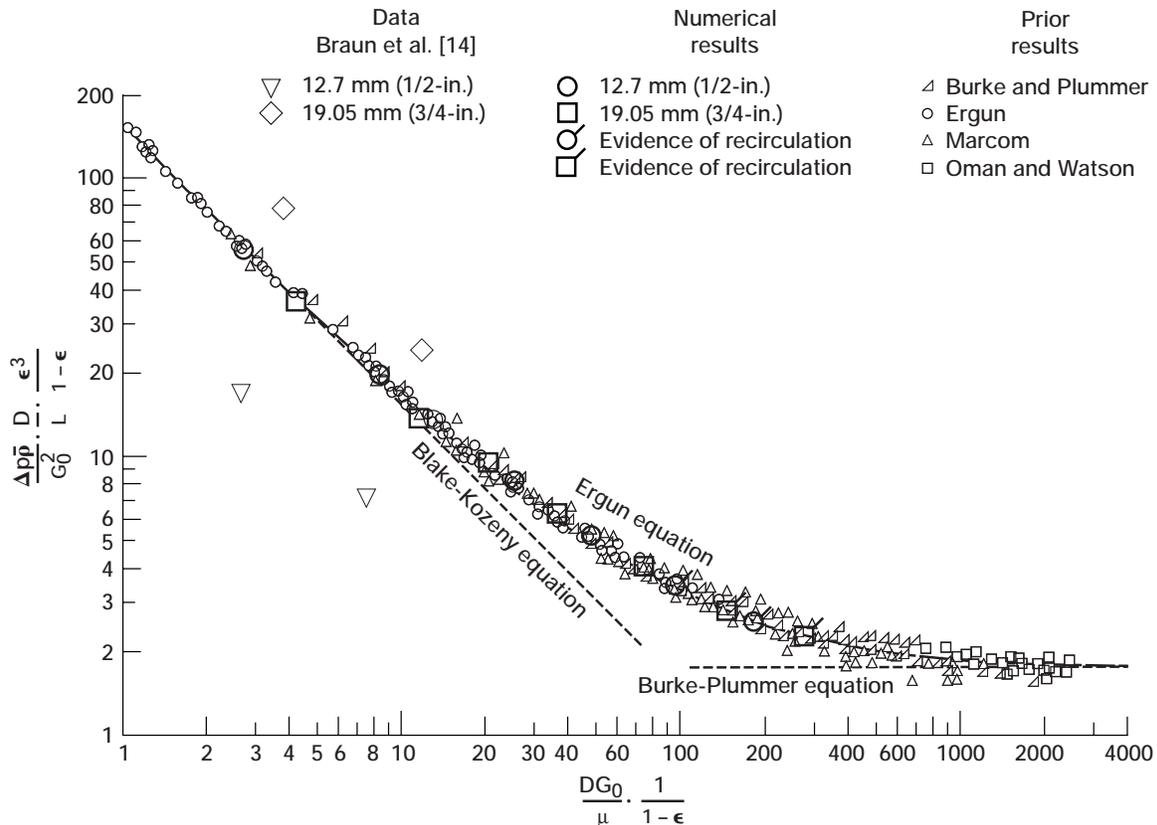|	Inlet velocity, m/s (flow rate, gal/min)						
	0.016 (1)	0.048 (3)	0.08 (5)	0.144 (9)	0.288 (18)	0.576 (36)	1.152 (72)
Pressure drop, MPa/m							
Sphere diamter, 12.7 mm (1/2 in.) Ergun relation	0.042 .043	0.138 .138	0.249 .243	0.507 .486	1.25 1.19	3.34 3.24	9.94 9.95
Difference, percent	3	0	–2.2	–4.3	–5.1	–2.9	0.1
Sphere diameter, 19.05 mm (3/4 in.) Ergun relation	0.0192 .0196	0.065 .064	0.12 .116	0.252 .24	0.653 .625	1.848 1.827	5.738 5.964
Difference, percent	1.8	–1.5	–3.8	–5.1	–4.5	–1.2	3.8

Figure 11.—Numerical and experimental results superimposed on a sketch illustrating the general behavior of the Ergun-relation (Bird et al. [4]).

Departures of the experimental data from the Ergun-locus are most likely due to difficulties in measuring the local pressure drops at the appropriate positions within the array and require further investigations. These figures, the video recording, and the experiments reveal that clear flow threads were established by the interstitial flow domain shapes. In general, the flow patterns were similar for the two flow rates and correlated well with the experimental pattern. The flow velocities (Reynolds numbers) were small enough that there were no major recirculation zones at tunnel inlet velocities below 0.6 m/s (flow rates below 36 gpm); incipient computational instabilities and vortical structures, figure 12, occurred above 1.15 m/s (flow rates above 70 gpm). These transition effects are being investigated. Some evidence of secondary vortical structures in the flow field was seen in the earlier flow

simulations by Athavale et al. [14] at fairly high Reynolds numbers (over 400).

Thermal Simulation Using Thermal Liquid Crystal (TLC)

For a set of experiments two liquid-crystal-coated spheres were introduced into an ordered but not regularly packed bed. Dissipated pump power slowly heated the circulated fluid, and distinct color banding illustrated regions of high thermal gradients near points of contact. The flows in these regions varied from zero to the free-stream flow thread, but near the surface the velocities were low. Upstream, the heat transfer was by convection; near the points of contact, conduction dominated; and downstream, wakes and rapid changes in curvature
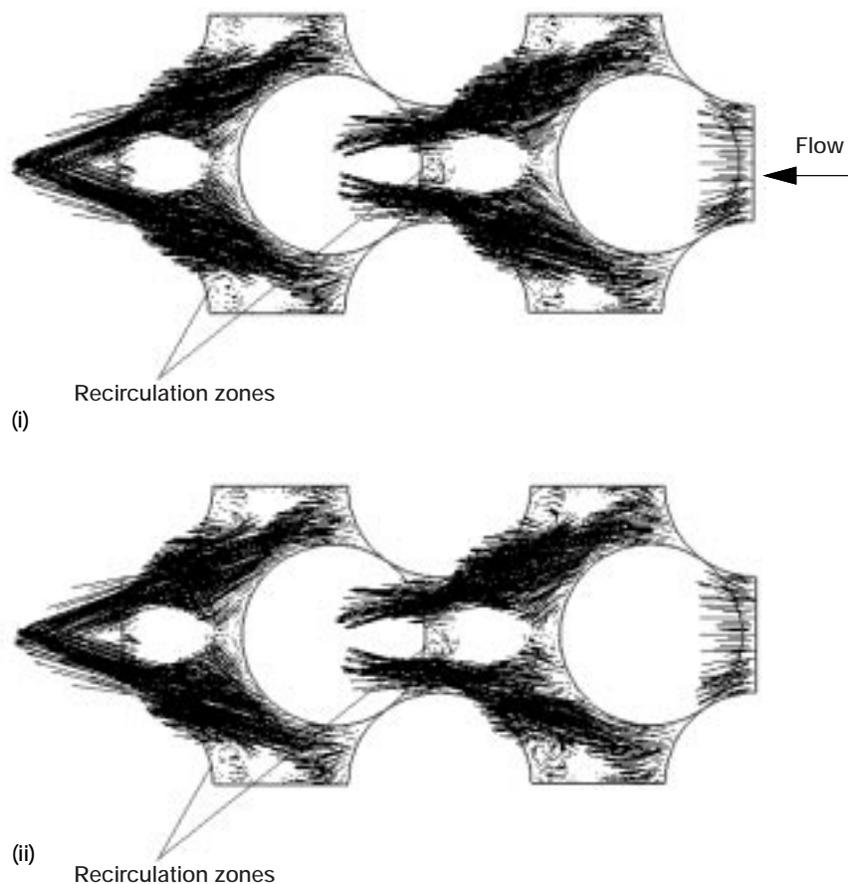
Figure 12a.—Velocity vector plots 12.7-mm-diameter 'cube', flow rate at:
(i) 136 liters/min (36 gal/min). (ii) 273 liters/min (72 gal/min).

provided mixed heat transfer. Distinct thermal variations outlined these regions.

Videorecording

The complexity of the flow field, whether virtual or experimental, became vivid through the video-recording. Visualization of the flow fields revealed flow threads, wakes, stagnation zones, and the strong influence of the wall-sphere interfaces. The tape is available in 1/2-in. VHS format. The essences of both the theoretically predicted flow threads and those observed experimentally can be visualized during a scan of the flow field from front to rear lateral walls. These flow threads weave through the packed array of spheres in the lateral direction, the direction of the bulk flow. Details of the flow boundary layer close to the wall and pro-

gressing through the matrix to the opposite wall are revealed. The videorecording can also be used to determine quantitative experimental information, such as the flow velocities, by using the FFFT technique [11,12] and comparing these to the virtual flows determined by the CFD solutions.

Summary

A videotape presentation is provided that enables the viewer to compare experimental and virtual computational fluid dynamic flows through packed beds of spheres or porous media. For the experiment the refraction indices of the oil working fluid and the spheres were closely matched so that only the boundaries of the physical spheres remained faintly visible to the eye and the cameras. The system fluid dynamics were made visible by seeding
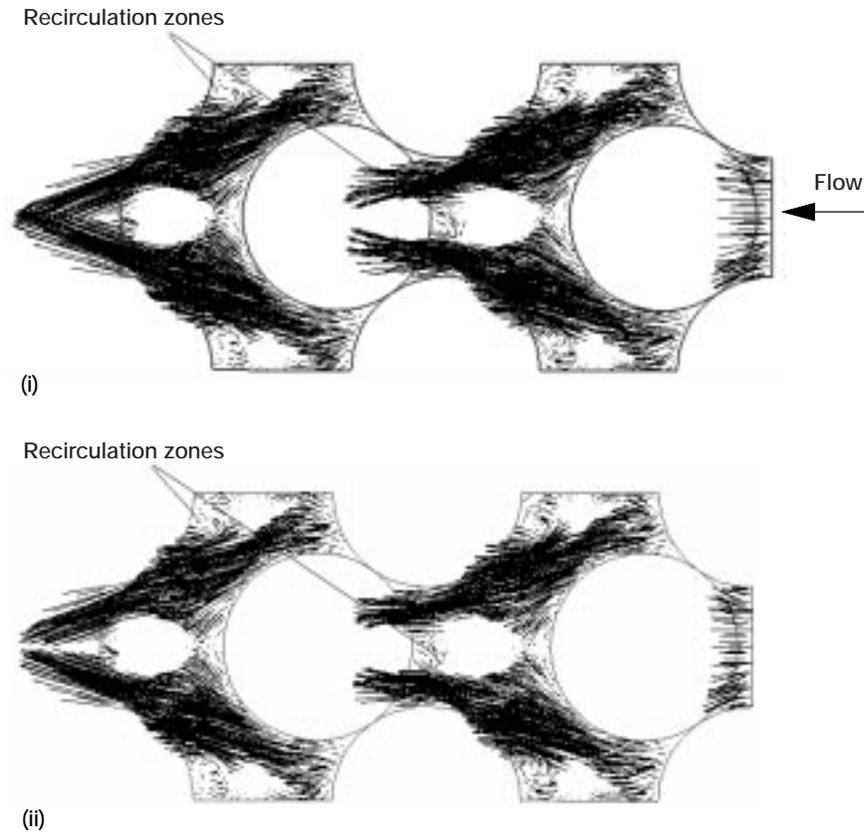
Figure 12b.—Velocity vector plots 19.05-mm-diameter 'cube', flow rate at:
(i) 136 liters/min (36 gal/min). (ii) 273 liters/min (72 gal/min).

the flow with aluminum oxide particles and illuminating the packed bed with a planar laser light sheet aligned in the direction of the bulk flow. The two-dimensional projection of the flow field was recorded at right angles to the bulk flow. As the planar light sheet traverses from the front wall to the rear wall of the tunnel and returns, completing one cycle, a three-dimensional image of the entire flow field can be visualized. The boundary interfaces between the working fluid and the spheres rendered the spheres black, permitting visualization of the planar circular interfaces in both the axial and transverse directions and providing direct visualization of the flow in complex interstitial spaces between the spheres within the bed. For the CFD virtual flows, simulations were performed with the flow direction at right angles to that used in the experiments to allow symmetry plane specifications. Even with this alteration for a 'cube' with face symmetries the flow patterns and threads were

similar to those found experimentally. Simulations with periodic conditions and higher tunnel inlet velocities are under way that will allow exact comparison.

The pressure drops per unit length in the packed bed were also calculated and compared with results from Ergun's theory for porous media, and good correlation between the two sets was obtained.

Flows were observed near the plane surfaces and within the set of spheres. The computational bed was regular, but the experimental bed was not as regularly aligned or uniformly ordered. Although the flow is truly three-dimensional and complex to describe, the most prominent finding was flow threads as computed in the representative 'cube' of spheres with face symmetry and conclusively demonstrated experimentally herein. The bulk of the flow field always tended to find natural flow paths, called threads, through the packed bed that are parallel and distinct. For a regular array the number of

such threads is represented by the open areas in the cross-sectional view of the flow field. Random packing and bed voids tended to disrupt the flow, creating some vortices. In one test liquid-crystal-coated spheres illustrated regions of poor heat transfer at the junctions of the spheres and wake effects.

References

[1] Hendricks, R.C., Lattime, S., and Braun, M.J., Athavale, M.M.: Experimental visualization of flows in packed beds of spheres. NASA TM–107365, 1997.

[2] Hendricks, R.C., Athavale, M.M., Braun, M.J., and Lattime, S.: Numerical flow visualization in basic- and hyper-cluster spheres. NASA TM–107361, 1997.

[3] Ergun, S.: Fluid flow through packed columns. Chemical Engineering Progress, vol. 43, pp. 89–94, Feb. 1952.

[4] Bird, R.B., Stewart, W.E., and Lightfoot, E.N.: *Transport phenomena*. John Wiley & Sons, New York, p. 200, 1960.

[5] Jolls, K.R., and Hanratty, T.J.: Transition to turbulence for flow through a dumped bed of spheres. Chemical Engineering Science, vol. 21, p. 1185, 1966.

[6] Karabelas, A.J.: Flow through regular assemblies of spheres. PhD Thesis, University of Illinois, Urbana, 1970.

[7] Wegner, T.H., Karabelas, A.J., and Hanratty, T.J.: Visual studies in a regular array of spheres. Chemical Engineering Science, vol. 26, pp. 59–63, 1971.

[8] Saleh, S., Thovert, J.F., and Adler, P.M.: Measurement of two-dimensional velocity fields in porous media by particle image displacement velocimetry. Experiments in Fluids, vol. 12, pp. 210–212, 1992.

[9] Rosenstein, H.D.: Nonlinear laminar flow in a porous medium. PhD Thesis, Case Western Reserve University, Cleveland, Ohio, 1980.

[10] Yarlagadda, A.P., and Yoganathan, A.P.: Experimental studies of model porous media fluid dynamics. Experimental Fluids, vol. 8, pp. 59–71, 1989.

[11] Braun, M.J., Batur, C., and Karavelakis, G.: Digital image processing through full flow field tracing (FFFT) in narrow geometries at low Reynolds numbers. Proceedings of First National Fluid Dynamics Congress, Cincinnati, Ohio, 1988.

[12] Braun, M.J., Hendricks, R.C., and Canacci, V.A.: Flow visualization in a simulated brush seal. Paper 90–GT–217, 35th ASME International Gas Turbine and Aeroengine Congress and Exposition, Brussels, Belgium, 1990.

[13] Athavale, M.M., and Przekwas, A.J.: SCISEAL: a CFD code for analysis of fluid dynamic forces in seals. NASA Workshop on Seals and Flow Code Development–1993, NASA CP–10136, 1994.

[14] Athavale, M.M., Przekwas, A.J., and Braun, M.J.: Flow and heat transfer analysis for packed beds on heated spheres, Part 1: Numerical computations. Final Report on Contract NAS3–25967, 1994.

[15] Anon.: *CFD-GEOM users manual*. CFD Research Corp., Huntsville, Alabama, 1997.

[16] Kudriavtsev, V.V., Hendricks, R.C., Braun, M.J, and Athavale, M.M.: Pressure drop design curves for brush seal applications. 33rd Joint Propulsion Conference, Seattle, Washington, AIAA 97–2635, 1997.

REPORT DOCUMENTATION PAGE

1. AGENCY USE ONLY *(Leave blank)*	2. REPORT DATE	3. REPORT TYPE AND DATES COVERED
	August 1998	Technical Memorandum

4. TITLE AND SUBTITLE

Virtual and Experimental Visualization of Flows in Packed Beds of Spheres Simulating Porous Media Flows

5. FUNDING NUMBERS

WU–910–30–11–00

6. AUTHOR(S)

R.C. Hendricks, M.M. Athavale, S.B. Lattime, and M.J. Braun

7. PERFORMING ORGANIZATION NAME(S) AND ADDRESS(ES)

National Aeronautics and Space Administration
Lewis Research Center
Cleveland, Ohio 44135–3191

8. PERFORMING ORGANIZATION REPORT NUMBER

E–11214

9. SPONSORING/MONITORING AGENCY NAME(S) AND ADDRESS(ES)

National Aeronautics and Space Administration
Washington, DC 20546–0001

10. SPONSORING/MONITORING AGENCY REPORT NUMBER

NASA TM—1998-207926

11. SUPPLEMENTARY NOTES

Prepared for the Eighth International Symposium on Flow Visualization cosponsored by the Universita di Napoli and Heriot Watt University, Sorrento, Italy, September 1–4, 1998. R.C. Hendricks, NASA Lewis Research Center; M.M. Athavale, CFD Research Corporation, Huntsville, Alabama 35805; S.B. Lattime, B&C Engineering, Akron, Ohio 44311; and M.J. Braun, University of Akron, Akron, Ohio 44325. Responsible person, R.C. Hendricks, organization code 5000, (216) 977–7507.

12a. DISTRIBUTION/AVAILABILITY STATEMENT

Unclassified - Unlimited
Subject Category: 34   Distribution: Nonstandard

This publication is available from the NASA Center for AeroSpace Information, (301) 621–0390.

12b. DISTRIBUTION CODE

13. ABSTRACT *(Maximum 200 words)*

A videotape presentation of flow in a packed bed of spheres is provided. The flow experiment consisted of three principal elements: (1) an oil tunnel 76.2 mm by 76.2 mm in cross section, (2) a packed bed of spheres in regular and irregular arrays, and (3) a flow characterization methodology, either (a) full flow field tracking (FFFT) or (b) computational fluid dynamic (CFD) simulation. The refraction indices of the oil and the test array of spheres were closely matched, and the flow was seeded with aluminum oxide particles. Planar laser light provided a two-dimensional projection of the flow field, and a traverse simulated a three-dimensional image of the entire flow field. Light focusing and reflection rendered the spheres black, permitting visualization of the planar circular interfaces in both the axial and transverse directions. Flows were observed near the wall-sphere interface and within the set of spheres. The CFD model required that a representative section of a packed bed be formed and gridded, enclosing and cutting six spheres so that symmetry conditions could be imposed at all cross-boundaries. Simulations had to be made with the flow direction at right angles to that used in the experiments, however, to take advantage of flow symmetry. Careful attention to detail was required for proper gridding. The flow field was three-dimensional and complex to describe, yet the most prominent finding was flow threads, as computed in the representative 'cube' of spheres with face symmetry and conclusively demonstrated experimentally herein. Random packing and bed voids tended to disrupt the laminar flow, creating vortices.

14. SUBJECT TERMS

Flow visualization; CFD; Porous media; Packed beds

15. NUMBER OF PAGES

21

16. PRICE CODE

A03

17. SECURITY CLASSIFICATION OF REPORT	18. SECURITY CLASSIFICATION OF THIS PAGE	19. SECURITY CLASSIFICATION OF ABSTRACT	20. LIMITATION OF ABSTRACT
Unclassified	Unclassified	Unclassified	